

# X-ray spectral evolution of low-mass X-ray binary GX 349+2

V. K. Agrawal, P. Sreekumar

*Space Astronomy & Instrumentation Division, ISRO Satellite Centre Bangalore-17*

*e-mail : vivekag@isac.ernet.in , ps Kumar@isac.ernet.in*

Released 2002 Xxxxx XX

## ABSTRACT

We present the results of a systematic investigation of spectral evolution in the Z source GX 349+2, using data obtained during 1998 with Proportional Counter Array (PCA) on-board the RXTE satellite. The source traced an extended normal branch (NB) and flaring branch (FB) in the color-color diagram (CD) and hardness-intensity diagram (HID) during these observations. The spectra at different positions of Z-track were best fitted by a model consisting of a disk blackbody and a comptonized spectrum. A broad (Gaussian) iron line at  $\sim 6.7$  keV is also required to improve the fit. The spectral parameters showed a systematic and significant variation with the position along the Z-track. The evolution in spectral parameters is discussed in the view of increasing mass accretion rate scenario, proposed to explain the motion of Z sources in the CD and HID.

**Key words:** accretion, accretion disc – binaries: close – stars: individual: GX 349+2 – stars: neutron – X-rays: stars – X-rays: general.

## 1 INTRODUCTION

Low Mass X-ray binaries (LMXBs) containing neutron stars are broadly divided into two classes: Z and atoll sources (Hasinger & van der Klis 1989). This classification is based on the shape of the path traced by these sources in the X-ray color-color diagram (CD) or hardness-intensity diagram (HID). Z-sources trace out a Z-type pattern in CD and HID, and have luminosities close to Eddington limit ( $L_{Edd}$ ). A Z-track consists of three parts, horizontal branch (HB), normal branch (NB) and flaring branch (FB). Atoll sources trace out a fragmented shape in CD. They have luminosities  $0.01-0.1 L_{Edd}$  and probably, have weaker magnetic fields than Z-sources (van der Klis 1995; Psaltis, Lamb & Miller 1995). It is widely believed that in Z-sources the inferred mass accretion rate increases along the Z-track from HB to FB (Hasinger et al. 1990). Similarly, in atoll sources inferred mass accretion rate increases along the fragmented path from the island state to upper part of the banana branch.

X-ray spectra of LMXBs can be described as the sum of soft and hard components. Two different approaches have been used to model these components. In the first case, the soft component is modeled by a single temperature blackbody corresponding to the hot surface of neutron star and a hard component corresponding to comptonized emission from the inner disk or boundary layer (White et al. 1986; White, Stella & Parmar 1988; Di Salvo et al. 2000, 2001). In the second approach, the soft component is described by a multicolor disk blackbody from accretion disk and the hard component is modeled by comptonized emission (Mitsuda et al. 1984, 1989; Di Salvo et al. 2002). Comparison of these models with observed data have shown that both the approaches require an additional broad iron  $K_{\alpha}$  line, arising from the ionized disk or from the accretion disk corona (ADC). Atoll sources

exhibit two distinct spectral states; namely hard and soft. In hard state their spectrum extends upto energies  $\gtrsim 100$  keV (Barret et al. 2000). The spectrum of Z sources is much softer, with cutoff energies of a few keV. In addition, a hard tail has been occasionally seen in the spectrum of the 5 Z sources (GX 5-1: Asai et al. 1994; GX 17+2: Di Salvo et al. 2000; GX 349+2: Di Salvo et al. 2001; Sco X-1: D’Amico et al. 2001; Cyg X-2: Frontera et al. 1998; Di Salvo et al. 2002).

UV/optical observations (Vrtilek et al. 1990) and correlated spectral and timing study of Z sources suggest (van der Klis 1995) that accretion rate increases along the Z-track from HB to FB. Modeling of X-ray spectra of Z sources also indicate that their motion in the CD is caused by variations in the inferred mass accretion rate (Psaltis, Lamb & Miller 1995). However, other possibilities also exist (van der Klis 2000). Thus, investigations of spectral evolution along the CD may provide an important clue to understand this scenario. The evolution of X-ray spectra of several Z sources have been investigated using BeppoSAX (GX 17+2: Di Salvo et al. 2000; GX 349+2: Di Salvo et al. 2001; Cyg X-2: Di Salvo et al. 2002). In GX 349+2, no appreciable change was observed in spectral parameters as source moved from NB to FB. Only, seed photon and electron temperature were slightly higher in FB than NB. Also, in GX 17+2 spectral parameters did not vary significantly from HB to NB. X-ray spectra of Cyg X-2 showed an interesting evolution along the Z-track (Di Salvo et al. 2002). It was found that as the source Cyg X-2 made a transition from HB to NB the inner disk temperature increased and at the same time inner rim of accretion disk moved inward. Also, optical depth of comptonized component systematically decreased and electron temperature increased as the source moved from HB to NB. The authors suggest that hardening of the soft blackbody component and softening of the hard comptonized

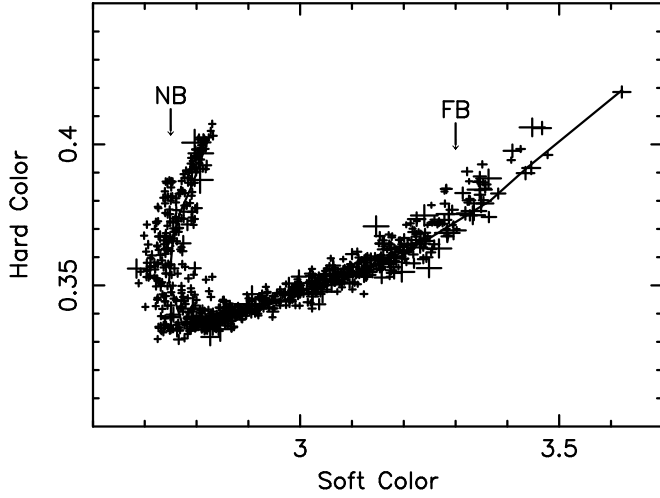


**Figure 1.** Color-color diagram of GX 349+2 for the January and September-October 1998 data sets. Soft color is count-rate-ratio in 3.5-6.4 keV and 2.0-3.5 keV energy ranges and hard color is that in energy bands 6.4-9.7 keV and 9.7-16.0 keV. The solid line in this figure represents an average Z-track passing through normal points. Each points is derived from a time bin size of 256s.

emission are probably responsible for HB to NB transition.

In this paper, we present the most detailed investigation of spectral evolution in GX 349+2 using extensive data set obtained with RXTE. The source traced the most complete CD during our observations (Zhang, Strohmayer & Swank 1998; Agrawal & Bhattacharya, 2003; O'Neill et al. 2002), providing an opportunity to study the spectral evolution in detail.

## 2 OBSERVATION

We analyzed public archival data obtained with PCA instrument on-board RXTE satellite. The data were collected during January and September-October, 1998. The total observation time with good data from PCA is  $\sim 220$  ks. The PCA consists of five identical proportional counter units with total effective area of  $\sim 7000$  cm<sup>2</sup> in the energy range 2-60 keV (Jahoda et al. 1996).

## 3 COLOR-COLOR DIAGRAM

The PCA standard-2 mode data, accumulated every 16s in the energy range 2-60 keV were used to create X-ray color-color diagram (CD) and Hardness-Intensity diagram (HID). The soft color is defined as the ratio of count rates in 3.5-6.4 keV and 2.0-3.5 keV energy ranges and hard color is defined as that in 9.7-16.0 keV and 6.4-9.7 keV energy ranges. The ‘rank number’ or ‘ $S_z$ ’ parameterization technique (Dieters & van der Klis 2000, and reference there in) was used to define the position of the source in CD. We selected the normal points in the CD in such a way that they form a smooth curve. The color-color points in the CD are projected onto this curve. The  $S_z$  parameter for each projected point was calculated by measuring their distance from NB/FB vertex ( $S_z = 2$ ) and end-point of the FB ( $S_z = 3$ ) were taken as reference points and rest of the Z curve was normalized according to the length of FB. The CD obtained from January and September-October observations of this source is shown in figure 1. The solid curve in figure 1 represents the approximate Z-track.

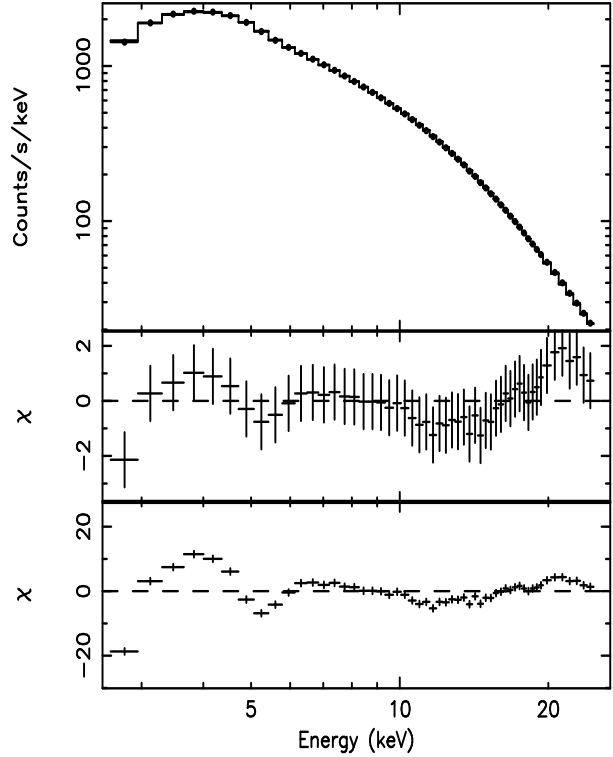


**Figure 2.** Count-rate spectrum and folded model (power-law) for the Crab is shown in panel 1. The residuals in the unit of  $\sigma$  are shown in panel 2 (a systematic error of 1 % is included) and panel 3 (without an inclusion of systematic error). The filled circle represent the observed count rate spectrum.

## 4 SPECTRAL ANALYSIS

The standard-2 mode PCA data were used to create the spectra in the energy range 2.5-25.0 keV. **The new *cmbrightvle* model file “pca\_bkgd\_cmbrightvle\_e3v20020201” for epoch 3 was used to calculate the PCA background.** We used the observation (from obsid 30133-01-02-00 to 30133-01-02-08) of Crab Nebula to derive the level of uncertainty in the PCA response matrix. Fitting the Crab spectrum (in the energy range 2.5-25.0 keV) to a power-law with photon-index ( $\Gamma$ ) =  $2.185 \pm 0.005$  provided a reduced  $\chi^2$  ( $\chi^2_\nu = \chi^2/d.o.f$ ) of 911/51. But, an inclusion of 1% systematic error reduced the value of  $\chi^2_\nu$  to 41/51. Hence, a systematic error of 1% was added to all the spectra to take into account the uncertainty in the PCA response matrix. In figure 2, the effect of PCA systematics on the Crab spectrum has been shown.

We divided the NB into 5 intervals and FB into 8 intervals to make an extensive investigation of spectral evolution in the source GX 349+2 along the Z-track. The source and background spectra within each interval were added separately to form a cumulative source and background spectrum. The background subtracted energy spectrum in the 2-25 keV range were fitted using a two-component model. The multi-temperature blackbody (**diskbb** in XSPEC, Mitsuda et al. 1984) or a single temperature blackbody (**bbody** in XSPEC) was used to describe the soft component. To model the hard component, comptonization models **compst** (Sunyaev & Titarchuk 1980) and **comptt** (Titarchuk 1994) of XSPEC were used. We find that **diskbb+comptt** model provided a better fit ( $\chi^2_\nu = 133/48$ ) to the spectrum at upper NB (NB1) compared to **bbody+comptt** model ( $\chi^2_\nu = 158/48$ ). The **diskbb+compst** model provides a poor fit to the spectrum for in-

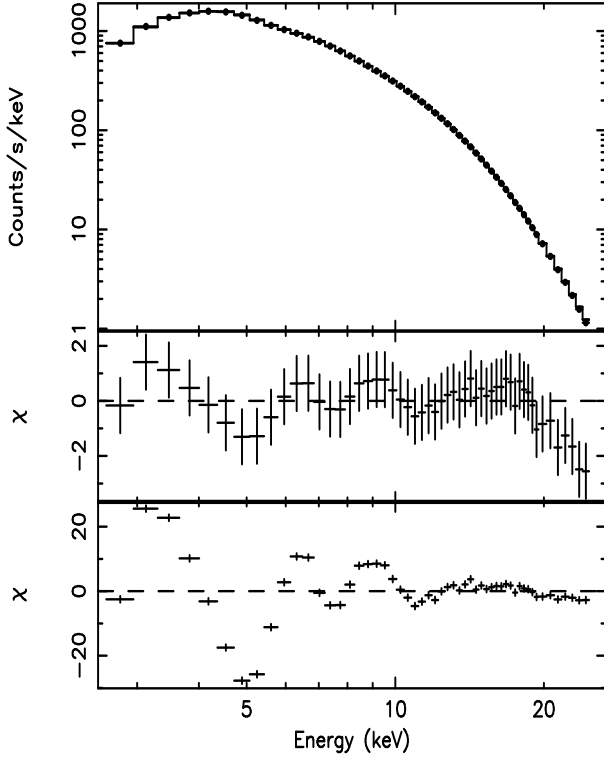


**Figure 3.** Count-rate spectrum with folded model (**diskbb+comptt+gauss+pl**) for the interval NB2 is shown in panel 1. The residuals in the unit of  $\sigma$  are shown in panel 2 (a systematic error of 1 % is included) and panel 3 (without an inclusion of systematic error). The filled circles represent the observed count rate spectrum.

interval NB1 ( $\chi^2_\nu \sim 643/49$ ). It is to be noted that, in our case the temperature of diskbb component is nearly coinciding with lower energy range of the detector and hence **diskbb** and **bbody** model cannot be discriminated clearly. The analysis of X-ray bursts from GX 17+2 has suggested that the soft component comes from the optically thick accretion disk (Kuulkers et al. 2002). Therefore, we chose **diskbb+comptt** model to describe the 2.5-25.0 keV spectra at various parts of Z-track. A Gaussian emission line at  $\sim 6.7$  keV is required to improve the fit to the spectra for all the positions on the Z-track. Addition of this line decreased  $\chi^2_\nu$  from 133/48 to 30.7/45 for the spectrum of NB1 (probability of chance improvement of fit is  $\sim 2.3 \times 10^{-14}$ ). The count rate spectrum for the source GX 349+2 (during interval NB2) in the energy range 2.5-25 keV and best-fit to it are shown in the panel 1 of figure 3. The residuals in the unit of sigma, with and without inclusion of systematic error are shown in panel 2 and 3 respectively.

## 5 RESULTS AND DISCUSSION

The values of best fit spectral parameters are given in Table 1 (for NB) and Table 2 (for FB). The diskbb model represents the soft emission expected from the optically thick accretion disk and provides two important disk parameters, color temperature ( $T_{col}$ ) of inner disk and inner disk radius ( $R_{in}$ ). The inner disk radius  $R_{in}$  is expressed by:

$$\left(\frac{R_{in}}{km}\right) = \frac{\sqrt{K} \times \left(\frac{D}{10 \text{ kpc}}\right)}{\sqrt{\cos \theta}} \quad (1)$$

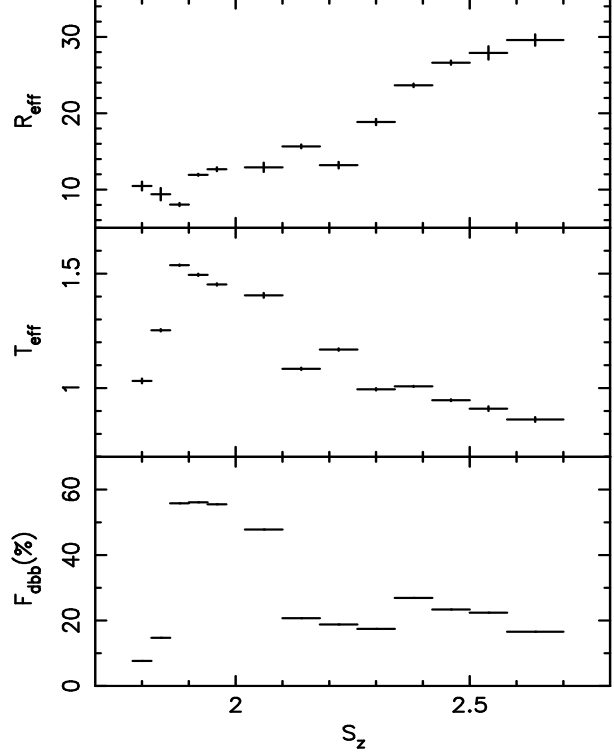


**Figure 4.** Variation of the best-fit **diskbb** parameters as a function of position (in terms of  $S_z$  parameter) along the Z-track. The inner disk temperature  $T_{eff}$  is given in keV and the inner disk radius  $R_{eff}$  is given in km.  $F_{dbb}$  (in %) gives percentage contribution of **diskbb** flux to the total flux (in the energy range 2.5-25.0 keV).

In this expression  $K$  is the disk blackbody normalization,  $D$  is the distance to the source in kpc, and  $\theta$  is the inclination of the accretion disk. Distance of the source GX 349+2 is uncertain and probably lies in the range 5-10 kpc (Cooke and Ponman 1991; Christian and Swank 1997; van Paradijs & McClintock 1994). Optical observation suggests that if GX 349+2 is a LMXB (mass of companion  $< 2M_\odot$ ) then inclination should be  $\theta > 25^\circ$  for the neutron star of mass  $< 2M_\odot$  (Wachter & Margon 1996). X-ray properties of Z-sources suggest that there are two different classes of Z-sources (Kuulkers et al. 1994; Kuulkers, van der Klis and Vaughan 1996): Cyg-like (Cyg X-2, GX 5-1, Sco X-1) and Sco-like sources (Sco X-1, GX 349+2, GX 17+2). One of the best studied Cyg-like source Cyg X-2 has an inclination  $\theta \sim 60^\circ$  (Orosz and Kuulkers 1999). As, it has been proposed that Sco-like sources are being viewed at lower inclination than Cyg-like sources (Kuulkers et al. 1994; Kuulkers, van der Klis and Vaughan 1996), for the source GX 349+2 inclination should be  $25^\circ < \theta < 60^\circ$ . Therefore we assume a mean inclination  $\theta = 45^\circ$  and distance  $D = 7.5$  kpc for GX 349+2 to derive its inner disk radius. It is to be noted that a different choice of inclination and distance in the range specified above will scale the inner disk radius by a factor of 0.59 to 1.58. However, as the inner disk radius for all the positions on the Z-track are scaled by the same amount, an overall trend of the change in the inner disk radius will not be affected.

In the multicolor disk model the local emission is described by blackbody spectrum (Shakura & Sunyaev 1973). However, it is expected that in the inner region of the disk, opacity due to electron scattering dominates over that due to absorption processes. In

this case the local spectrum can be significantly modified by comptonization and can be approximated by,

$$I_\nu = \frac{1}{f^4} B_\nu(T_{col}) \quad (2)$$

where,  $f = \left(\frac{T_{col}}{T_{eff}}\right)$  is the spectral hardening factor,  $T_{col}$  is the color temperature of inner disk,  $T_{eff}$  is the effective temperature of inner disk,  $\nu$  is the frequency of radiation,  $B_\nu(T_{col})$  is the Planck function (Ebisawa et al. 1994). The effective radius and temperature of inner disk is given by,

$$R_{eff} = f^2 R_{in} \quad (3)$$

$$T_{eff} = \frac{T_{col}}{f} \quad (4)$$

By solving the vertical structure and radiative transfer equation of the disk, Shimura & Takahara (1995) showed that for viscosity parameter  $\alpha \sim 0.1$ , luminosity close to Eddington limit and mass of the compact object  $1.4-10 M_\odot$  the soft emission from disk can be described by equation 2 with spectral hardening factor  $f=1.9 \pm 0.1$ .

The variation in the parameters of soft component as a function of  $S_z$  parameter is shown in figure 4. Our study revealed that  $T_{eff}$  increased from  $\sim 1$  keV to  $\sim 1.5$  keV as source moved from upper to middle part of NB, i.e in the direction of increasing  $S_z$ . Increase in  $T_{eff}$  can be interpreted in terms of inward motion of accretion disk with increasing accretion rate. In fact inner disk radius  $R_{eff}$  was found to decrease from upper NB ( $\sim 10.5$  km) to middle NB ( $\sim 8.0$  km). As source moved further from middle NB to upper FB,  $T_{eff}$  decreased from  $\sim 1.5$  keV to  $\sim 0.86$  keV. At the same time  $R_{eff}$  increased from  $\sim 12$  km to  $\sim 30$  km. This suggests that inner rim of accretion disk moves outward again with increasing mass accretion rate.

As mentioned earlier, **diskbb** radiation is emitted by optically thick matter, which is in Keplerian flow. Since the radiation drag force exerted by radiation coming from the neutron star can remove significant angular momentum from the gas in Keplerian flow, radial flow starts a few stellar radii above the neutron star surface. The inner edge of the accretion disk can be taken as the point at which disk-flow ends and radial flow starts. Note that the intensity of radiation will be attenuated exponentially ( $\exp^{-\tau_r}$ , where  $\tau_r$  is the radial optical depth) as it passes through disk. Therefore radiation drag cannot remove any angular momentum beyond a certain distance ( $R_{aml}$ ) from the central compact object and supersonic radial flow is possible only within radius  $R_{aml}$  (Miller, Lamb & Psaltis 1998; Miller & Lamb 1996). This radius is obtained by setting  $\tau_r = 5$  (since most of the radiation will be attenuated beyond this optical depth). Since radial flow probably begins at the inner edge of the accretion disk,  $R_{aml}$  should be very close to  $R_{eff}$ , i.e.,  $R_{aml} \approx R_{eff}$ . Radial optical depth of accreting matter is given by equation 5 of Miller, Lamb & Psaltis (1998), which is

$$\tau_r = \frac{\sigma_T \dot{M}}{4\pi m_p} \int_R^r \frac{[1 - v^{\hat{r}}(r')]^{-1}}{\gamma_r(r') \gamma(r')} \frac{(1 - 2M/r')^{-1}}{r' h(r') v^{\hat{r}}(r')} dr'. \quad (5)$$

In this expression,  $\dot{M}$  is the mass accretion rate through the inner disk,  $\sigma_T$  is the Thomson scattering cross section,  $v^{\hat{r}}(r')$  is the radial velocity,  $h(r')$  is the half-thickness of disk,  $\gamma_r = [1 - (v^{\hat{r}})^2]^{-1/2}$ ,  $\gamma = [1 - v^{\phi 2} - v^{\hat{r} 2}]^{-1/2}$ , where  $v^{\phi}$  is azimuthal velocity of accretion flow. Note that in all the expressions of this section we have used units such that  $c = G = 1$ , where  $c$  is the speed of light and  $G$  is gravitational constant. By substituting  $\tau_r = 5$  and solving

equation 1 for radius (see equation 6 of Miller, Lamb & Psaltis (1998)) one can get

$$R_{eff} \approx R + 5 \left( \frac{\dot{M}}{0.01 \dot{M}_E} \right)^{-1} \left( \frac{R}{10 \text{ km}} \right) \left( \frac{v^{\hat{r}}}{0.1c} \right) \left( \frac{h/R}{10^{-2}} \right) \text{ km.} \quad (6)$$

From equation 6, it is clear that inner disk radius will decrease with increasing accretion rate. This explains decrease of inner disk radius seen from upper NB to middle NB. However equation 6 cannot explain the increase of inner disk radius from lower NB to upper part of FB. In this part of CD (from lower NB to upper FB) the source is supposed to be super-Eddington and hence gravitational pressure cannot support the radiation pressure. This will lead to an outflow in this part of the Z-track. It should be noted that equation 5 and 6 do not take into account the presence of outflow. The presence of outflow can remove the matter from radial inflow and can dump it into a hot central corona above the inner disk. This will lead to a reduction in the density of radial flow and hence, in radial optical depth. A decrease in the optical depth of radial flow will cause radiation to penetrate further inside the disk and hence the inner rim of the disk will shift outward (i.e.,  $R_{eff}$  will increase). Also, if a fraction of matter from radial inflow is pumped in to a hot corona then the optical depth of this corona will increase. In fact optical depth of the corona is found to increase along the FB where most likely  $\dot{M} > \dot{M}_{Edd}$ .

The contribution of the soft component ( $F_{dbb}$ ) to the total flux increases from  $\sim 8\%$  to  $56\%$  as the source moves from upper to lower NB. Again from lower part of NB to upper FB, the soft emission decreased from  $\sim 56\%$  to  $17\%$ . The variation in the soft component can be explained in terms of variations in the geometry of inner accretion disk with mass accretion rate. An inward motion of disk (from upper to middle NB) increased the area, emitting the soft component. As a result soft disk emission also increased. Similarly, an outward motion of disk (from lower NB to upper FB) caused a decrease in the soft disk flux.

The comptonized spectrum is produced by upscattering of soft photons (described by the Wien spectrum at  $\sim 1$  keV) by hot electrons in the central hot corona or boundary layer. Our analysis showed that parameters of the comptonized spectrum evolved significantly as the source moved along the Z-track (see figure 5). The electron temperature  $T_e$  of comptonizing plasma cloud increased from  $\sim 2.7$  keV to  $3.2$  keV along the NB. At the same time optical depth  $\tau$  of the plasma cloud decreased from  $\sim 5.6$  to  $2.8$ . Probably, increased heating of the central corona caused by increase in the incident flux reduces the density of corona and hence, decrease  $\tau$ . A decrease in  $\tau$  leads to a reduction in relative energy gain of the comptonization process, given by comptonization parameter  $y = \frac{4T_e}{m_e c^2} \tau^2$  (where  $m_e c^2$  is the rest mass of the electron), from upper to lower part of NB. Other possibility is that a slow collapse of the central corona to a geometrically thin accretion disk, leaving low density plasma cloud above the accretion disk (Di Salvo et al. 2002) may lead to a decrease in optical depth. In this case same amount of matter will be accreted on a smaller area (a strip around neutron star). This will cause an increase in seed photon temperature. In fact seed photon temperature  $T_W$  increased slowly from  $0.79 \pm 0.01$  keV to  $0.90 \pm 0.02$  keV along the NB. However, it is not clear that why a central corona should collapse to a geometrically thin disk. As source moved further from NB/FB vertex to upper FB,  $T_e$  decreased from  $\sim 3.3$  keV to  $2.6$  keV and  $\tau$  increased from  $\sim 3.2$  to  $6.4$ . In the FB, the radiation pressure is expected to be very high and dominant over gravitational pressure. Therefore, probably due to effect of radiation pressure, an outflow begins near the inner part of disk, creating a density enhancement in the hot corona above

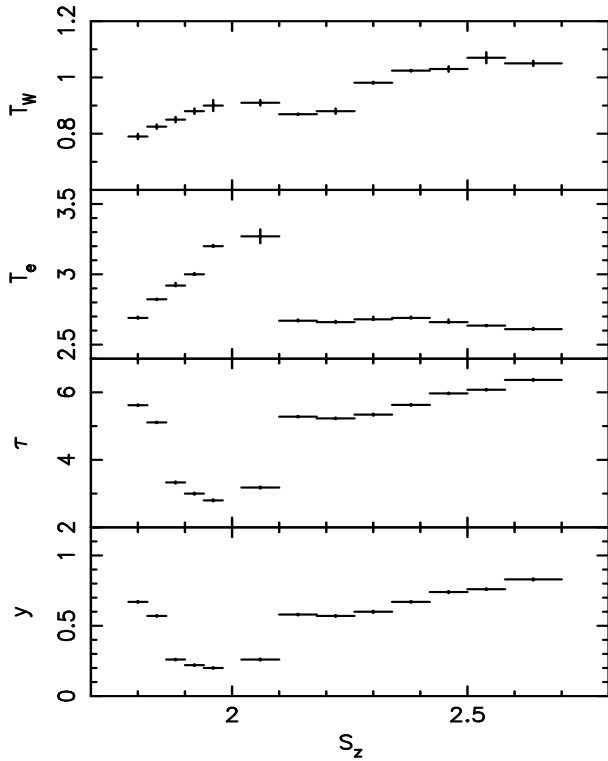


**Figure 5.** Variation in the best-fit *compTT* parameters as a function of position (in terms of  $S_z$  parameter) along the Z-track. Electron temperature  $T_e$  and seed photon temperature  $T_W$  are given in the unit of keV.

the inner disk and hence causing optical depth to increase along the FB. The comptonization parameter  $y$  also increases along the FB due to increase in optical depth.

The results of Di Salvo et al. (2001) on the source GX 349+2 from BeppoSAX data are different from our results. In their work, the whole Z-track was divided into two intervals; NB and FB. The spectra of FB and NB were best fitted with **body+compTT+power-law+Gaussian-lines**. As the source GX 349+2 moved from NB to FB temperature of the blackbody component slightly increased from  $0.51 \pm 0.01$  keV to  $0.59 \pm 0.02$  keV. At the same time optical depth of the comptonizing cloud decreased from  $11.7 \pm 0.4$  to  $10.5 \pm 0.5$  and electron temperature increased from  $2.65 \pm 0.05$  keV to  $2.95 \pm 0.07$  keV. The comptonization parameter  $y$  was  $\sim 2.84$  in the NB and  $\sim 2.54$  in the FB. Our results show that diskbb component is harder in the NB ( $T_{eff} = 2.75 \pm 0.01$ ) than FB ( $T_{eff} = 1.95 \pm 0.01$ ) and comptonized emission in the NB is soft ( $y \sim 0.38$ ) compared to that in the FB ( $y \sim 0.63$ ). **There may be two possible reasons behind the differences seen between our results and those of Di Salvo et al. (2001). First, they have used a model which is different from that used in our work. Second, they have used different energy ranges to model the NB (0.1-200 keV) and FB (1.8-200 keV) spectra as LECS data were not available during the flaring state.**

We calculated the radius of seed photon emitting region ( $R_W$ ) using expression,  $R_W = 3 \times 10^4 D \sqrt{\frac{F_{bol}}{1+y}} / (T_W)^2$  as given by

In 't Zand et al. (1999). Here,  $D$  is the distance in kpc,  $F_{bol}$  is the unabsorbed comptonized flux in  $ergs s^{-1} cm^2$ ,  $y$  is comptonization parameter and  $T_W$  is seed photon temperature in keV. The Wien radius  $R_W$  was  $\sim 30$ -48 km in the NB and  $\sim 30$ -40 km

in the FB. These values are considerably larger than that reported previously (Di Salvo et al. 2001).

We found a strong broad iron line at energies  $\sim 6.7$  keV, with width  $\sim 0.7$ -1.4 keV. It is to be noted that iron line was **stronger** in the FB (eq. width = 154-295) than NB (eq. width = 97-210). This behavior of GX 349+2 is just opposite to that exhibited by it during earlier observations (Di Salvo et al. 2001). We also note that in our case observed iron line is much stronger.

Even though X-ray intensity decreases or remains almost constant along the NB, it is generally believed that accretion rate increases along the Z-track. This arguments mostly relies upon two observational facts. First, UV and optical flux increases along the Z-track from HB to FB (Vrtilek et al. 1990; van Paradijs et al. 1990). UV and optical fluxes are thought to be better indicator of accretion rate than the X-ray flux (Hasinger et al. 1990). Second, frequency of Horizontal-Branch-Oscillation (HBO) and kHz quasi-periodic-oscillation (QPO) increases from HB to NB (van der Klis 2000, and reference there in). In almost all the models, frequency of these two oscillations is directly proportional to accretion rate (Lamb et al. 1985; Psaltis et al. 1999; Miller, Lamb & Psaltis 1998; Stella, Vietri & Morsink 1999). However, there are a few recent results which indicate that increasing accretion rate scenario may not be the true story (Homan et al. 2002) and motion along Z-track is caused by variation in the inner disk radius (van der Klis 2000). Our systematic investigation of spectral evolution showed that the motion of the source along the Z-track can be explained by variation in two emission components; soft disk emission and hard comptonized spectrum. The motion of the source along the NB (i.e softening of spectra) is caused by an increase in disk contribution and a decrease in degree of comptonization. Similarly, a decrease in the contribution of the soft component and an increase in Compton parameter  $y$  seems to be responsible for the motion of the source along the FB. As discussed earlier, the above changes in the soft component and in the comptonized spectrum are expected if accretion rate is increasing along the Z-track. Hence, our results seems to be in the favor of the scenario in which motion of the source along the Z-track is caused by variations in the accretion rate.

## 6 CONCLUSION

In this paper, we have carried out a detailed study of spectral evolution in the source GX 349+2 using RXTE data. During our observations the source is found both in the NB and FB. The continuum spectra at different positions of Z-track are well described by a disk blackbody and a comptonized component. We explain the evolution of parameters of both soft and hard components in terms of variations in the mass accretion rate along the Z-track. This study suggests that a systematic increase in the strength of soft component and a decrease in comptonization parameter  $y$  are responsible for the motion of the source along the NB. Similarly, a decrease in soft disk emission and increase in the  $y$  parameter may cause the source to move along the FB.

## ACKNOWLEDGMENTS

This work has made use of High Energy Astrophysics Science Archive Research Center (HEASARC) facility at NASA-Goddard Space Flight Center. We are thankful to the anonymous referee for his useful suggestions.

## REFERENCES

- Agrawal V. K., Bhattacharya S., 2003, *A&A*, 398, 223
- Asai K. et al., 1994, *PASJ*, 46, 479
- Barret D., Olive J.F., Boirin L., Done C., Skinner G.K., Grindlay J.E., 2000, *ApJ*, 533, 329
- Cooke B.A., Ponman T.J., 1991, *A&A*, 244, 358
- Christian D.J., Swank J.H., 1997, *ApJS*, 109, 177
- Di Salvo T. et al., 2000, *ApJ*, 544, L119
- Di Salvo T., Robba N.R., Iaria R., Stella L., Burderi L., Israel G.L., 2001, *ApJ*, 554, 49
- Di Salvo T. et al., 2002, *A&A*, 386, 535
- Dieters S.W., van der Klis M., 2000, *MNRAS*, 311, 201
- D'Amico F., Heindl W.A., Rothschild R.E., Gruber D.E., 2001, *ApJ*, 547, L147
- Ebisawa K. et al., 1994, *PASJ*, 46, 375
- Frontera F., Dal Fiume D., Malaguti G., et al., 1998, *Nuclear Physics B (Proc. Suppl.)*, 69, 286
- Hasinger G., van der Klis M., 1989, *A&A*, 225, 79
- Hasinger G., van der Klis M., Ebisawa K., Dotani T., Mitsuda K., 1990, *A&A*, 235, 131
- Homan J., van der Klis M., Jonker P.G., Wijnands R., Kuulkers E., Mendez M., Lewin W.H.G., 2002, *ApJ*, 568, 878
- In 't Zand J.J.M. et al., 1999, *A&A*, 345, 100
- Jahoda K., Swank J.H., Giles A.B., Stark M.J., Strohmayer T., Zhang W., Morgan, E. H., 1996, *SPIE*, 2808, 59
- Kuulkers E., van der Klis M., Oosterbroek T., Asai K., Dotani T., van Paradijs J., Lewin W.H.G., 1994, *A&A*, 289, 795
- Kuulkers E., van der Klis M., Vaughan B.A., 1996, *A&A*, 311, 197.
- Kuulkers E., Homan J., van der Klis M., Lewin W.H.G., Mendez M., 2002, *A&A*, 382, 947
- Lamb F.K., Shibasaki N., Alpar M.A., Shaham J., 1985, *Nature*, 317, 681
- Miller M.C., Lamb F.K., Psaltis D., 1998, *ApJ*, 508, 791
- Miller M.C., Lamb F.K., 1996, *ApJ*, 470, 1033
- Mitsuda K. et al., 1984, *PASJ*, 36, 741
- Mitsuda K., Inoue H., Nakamura N., Tanaka Y., 1989, *PASJ*, 41, 97
- O'Neill P.M., Kuulkers E., Sood R.K., van der Klis M. 2002
- Orosz Jerome A., Kuulkers E., 1999, *MNRAS*, 305, 132.
- Psaltis D., Lamb F.K., Miller G.S., 1995, *ApJ*, 454, L137
- Psaltis D. et al., 1999, *ApJ*, 520, 763
- Shakura N.I., Sunyaev R.A., 1973, *A&A*, 24, 337
- Shimura T. & Takahara F., 1995, *ApJ*, 445, 780
- Stella L., Vietri M., Morsink S.M., 1999, *ApJ*, 524, L63
- Sunyaev R.A., Titarchuk L.G., *A&A*, 1980, 86, 121
- Titarchuk L., 1994, *ApJ*, 434, 570
- van der Klis M., 1995, in Lewin W.H.G., van Paradijs J., van den Heuvel E.P.J., eds, *Rapid Aperiodic Variability in X-ray Binaries*. Cambridge University Press, Cambridge, p. 252
- van der Klis M., 2000, *AR&A*, 38, 717
- Vrtilek S.D., Raymond J.C., Garcia M.R., Verbunt F., Hasinger G., Kurster M., 1990, *A&A* 235, 162
- van Paradijs J. et al., 1990, *A&A*, 235, 156
- van Paradijs J., McClintock J.E., 1994, *A&A*, 290, 133
- Wachter S., Margon B., 1996, *AJ*, 112, 2684
- White N.E. et al. 1986, *MNRAS*, 218, 129
- White N.E., Stella L., Parmar A.N., 1988, *ApJ*, 324, 363
- Zhang W., Strohmayer T.E., Swank J.H. 1998, *ApJ*, 500, L167.

**Table 1.** Results of diskbb+comptt+gauss fit to the NB spectra of GX 349+2 in the 2.5-25.0 keV energy range. For each spectrum the range of  $S_z$  is given in the bracket. Errors on the best fit parameters are calculated by using  $\Delta\chi^2 = 1$  (68% confidence)

Para.	NB1 (1.80±0.02)	NB2 (1.84±0.02)	NB3 (1.88±0.02)	NB4 (1.92±0.02)	NB5 (1.96±0.02)
$T_W$ (keV)	0.79±0.01	0.825±0.008	0.85±0.01	0.88±0.01	0.90±0.02
$T_e$ (keV)	2.69 <sup>+0.01</sup> <sub>-0.004</sub>	2.822±0.004	2.92±0.02	3.00±0.01	3.20±0.01
$\tau$	5.62±0.02	5.11±0.01	3.33±0.03	3.00±0.03	2.80±0.03
$R_W$ (km)	48.35±2.2	44.07±1.41	22.71±1.1	29.97±1.35	29.28±1.05
$y$	0.67±0.006	0.57±0.003	0.26±0.005	0.22±0.005	0.20±0.004
$T_{eff}$ (keV)	1.03±0.01	1.25±0.005	1.54±0.003	1.49±0.005	1.45±0.005
$R_{eff}$ (km)	10.47±0.58	9.40±0.81	8.04±0.21	11.94±0.14	12.67±0.26
$F_{dbb}$ (%)	7.64	14.7	55.80	56.10	55.51
$E_l$ (keV)	6.76±0.2	6.89 <sup>+0.27</sup> <sub>-0.16</sub>	6.80±0.2	6.78±0.16	6.80±0.14
$\sigma_l$ (keV)	0.77 <sup>+0.25</sup> <sub>-0.14</sub>	0.61±0.34	0.72±0.15	0.73 <sup>+0.26</sup> <sub>-0.11</sub>	0.68 <sup>+0.23</sup> <sub>-0.11</sub>
Eq. Width (eV)	155	97	142	184	210
$\chi^2(d.o.f)$	30.7 (45)	31.0 (45)	32.8 (45)	31.0 (45)	36.0 (45)

**Table 2.** Results of diskbb+comptt+gauss fit to the FB spectra of GX 349+2 in the 2.5-25.0 keV energy range. For each spectrum the range of  $S_z$  is given in the bracket. Errors on the best fit parameters are calculated by using  $\Delta\chi^2 = 1$  (68% confidence)

Para.	FB1 (2.06±0.04)	FB2 (2.14±0.04)	FB3 (2.22±0.04)	FB4 (2.30±0.04)	FB5 (2.38±0.04)	FB6 (2.46±0.04)	FB7 (2.54±0.04)	FB8 (2.64±0.06)
$T_W$ (keV)	0.91±0.01	0.869±0.001	0.88±0.01	0.981±0.004	1.024±0.003	1.03±0.01	1.07±0.02	1.05 <sup>+0.015</sup> <sub>-0.005</sub>
$T_e$ (keV)	3.27±0.05	2.67±0.01	2.66±0.01	2.68±0.02	2.69±0.01	2.66±0.02	2.635±0.005	2.61±0.01
$\tau$	3.18±0.03	5.28±0.01	5.23±0.02	5.34±0.03	5.63±0.02	5.97±0.02	6.08±0.02	6.37±0.03
$R_W$ (km)	30.61±1.55	38.21±1.75	39.23±1.90	32.95±1.55	29.00±1.34	29.69±1.45	27.15±1.38	31.35±1.61
$y$	0.26±0.007	.58±0.005	0.57±0.005	0.60±0.008	0.67±0.005	0.74±0.008	0.76±0.006	0.83±0.008
$T_{eff}$ (keV)	1.40±0.01	1.08±0.005	1.16±0.006	0.99±0.004	1.01±0.003	0.95±0.004	0.91±0.01	0.86±0.01
$R_{eff}$ (km)	12.92±0.61	15.65±0.25	13.20±0.43	18.85±0.41	23.65±0.24	26.62±0.28	27.90±0.88	29.59±0.75
$F_{dbb}$ (%)	47.80	20.7	18.8	17.43	26.90	23.36	22.39	16.56
$E_l$ (keV)	6.74±0.01	6.73±0.06	6.78±0.04	7.02 <sup>+0.04</sup> <sub>-0.16</sub>	6.97 <sup>+0.05</sup> <sub>-0.15</sub>	6.94 <sup>+0.08</sup> <sub>-0.1</sub>	7.02 <sup>+0.3</sup> <sub>-0.2</sub>	6.9±0.18
$\sigma_l$ (keV)	0.76±0.05	0.80 <sup>+0.1</sup> <sub>-0.01</sub>	0.89±0.06	0.75±0.09	0.87±0.1	1.17±0.09	1.21±0.2	1.45±0.16
Eq. Width (eV)	207	227	241	154	161	222	205	295
$\chi^2(d.o.f)$	32.4 (45)	40.1 (45)	54.0 (45)	43.7 (45)	35.5 (45)	34.2 (45)	50.9 (45)	58.5 (45)